THE JOURNAL OF PHYSICAL CHEMISTRY LETTERS
A JOURNAL OF THE AMERICAN CHEMICAL SOCIETY

pubs.acs.org/JPCL

Letter

Bond Polarizability as a Probe of Local Crystal Fields in Hybrid Lead-Halide Perovskites

Yujing Wei,[‡] Artem G. Volosniev,[‡] Dusan Lorenc, Ayan A. Zhumekenov, Osman M. Bakr, Mikhail Lemeshko, and Zhanybek Alpichshev*

Cite This: *J. Phys. Chem. Lett.* 2023, 14, 6309−6314

Read Online

ACCESS | Metrics & More | Article Recommendations | Supporting Information

ABSTRACT: A rotating organic cation and a dynamically disordered soft inorganic cage are the hallmark features of organic-inorganic lead-halide perovskites. Understanding the interplay between these two subsystems is a challenging problem, but it is this coupling that is widely conjectured to be responsible for the unique behavior of photocarriers in these materials. In this work, we use the fact that the polarizability of the organic cation strongly depends on the ambient electrostatic environment to put the molecule forward as a sensitive probe of the local crystal fields inside the lattice cell. We measure the average polarizability of the C/N−H bond stretching mode by means of infrared spectroscopy, which allows us to deduce the character of the motion of the cation molecule, find the magnitude of the local crystal field, and place an estimate on the strength of the hydrogen bond between the hydrogen and halide atoms. Our results pave the way for understanding electric fields in lead-halide perovskites using infrared bond spectroscopy.

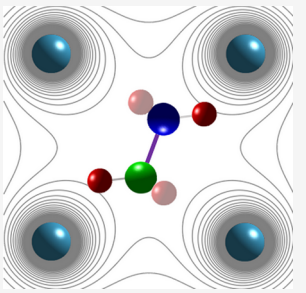

The efficiency of hybrid organic-inorganic lead-halide perovskite (HOIP)-based solar cells has recently nearly reached the levels of the state-of-the-art conventional Si-based devices.[1,2] On the microscopic level this impressive performance is contingent upon the presence of charged photocarriers that can travel unimpeded sufficiently far to reach the contacts of the photovoltaic element. The fact that this is indeed the case for lead-halide perovskites,[3−8] despite much higher defect concentration in HOIP samples as compared to standard photovoltaic materials such as Si,[9] is arguably the biggest puzzle in the field of perovskite research. While an exhaustive explanation is still lacking, the unexpectedly high efficiency of HOIPs, be it in photocarrier separation[10] or "neutralization" of defect centers,[11] suggests the pre-eminent role of charge screening. One possible source of such screening pointed out early on is the quasi-freely rotating polar organic cation occupying the A-site of HOIPs such as $CH_3NH_3^+$ (methylammonium, MA),[12−15] while others argue for the inorganic cage as the main responsible party.[16] In order to bring more clarity to this problem, a detailed understanding of the interaction between cation molecules and the surrounding cage is necessary. Unsurprisingly, this is not an easy task as while the former is semi-independent, the latter is soft, dynamically disordered, and highly anharmonic[17−22] with significant ionic conductivity[23] to the extent of being dubbed "plastic crystals" in some works.[24,25]

The very fact that the A-site cation retains its chemical autonomy inside the cage,[29−31] implies that the interaction between the two is mostly of an electrostatic nature.[32] To characterize the magnitude of this coupling, one needs therefore to be able to probe the local electric fields within the crystal, primarily the ones experienced by hydrogen atoms. Unfortunately, conventional tools such as nuclear quadrupole resonance spectroscopy[33−35] are not particularly suitable for this purpose as the lightest nuclei (proton, deuteron) have either no or small quadrupolar moment. In this light, we draw attention to the fact that in HOIPs, the A-site cation can itself act as a sensitive local probe of its immediate environment. Indeed, on the one hand, the cation is chemically decoupled from the inorganic cage and can be treated as a separate molecule, and on the other hand, it is often simple enough to allow for an exhaustive theoretical treatment.

In this work, we show that the ambient electrostatic environment can noticeably modify basic properties of the molecule such as its dynamic susceptibility using methylammonium in $MAPbBr_3$ as an example. We compare these theoretical results to the measured infrared polarizability of methylammonium, draw conclusions about the character of coupled cation-cage dynamics, put a numeric value on the effective local electric field experienced by the hydrogen atoms in methylammonium cation and estimate the strength of the hydrogen bond between H and Br atoms. These findings pave the way for employing infrared probes[36,37] for studying organic-inorganic crystal structures such as HOIPs.

Polarizability α_{ij} is a basic physical property of a molecule that relates the induced dipole moment, $\vec{p}$, of a molecule to the

Received: April 27, 2023
Accepted: June 26, 2023
Published: July 5, 2023

https://doi.org/10.1021/acs.jpclett.3c01158
J. Phys. Chem. Lett. 2023, 14, 6309−6314

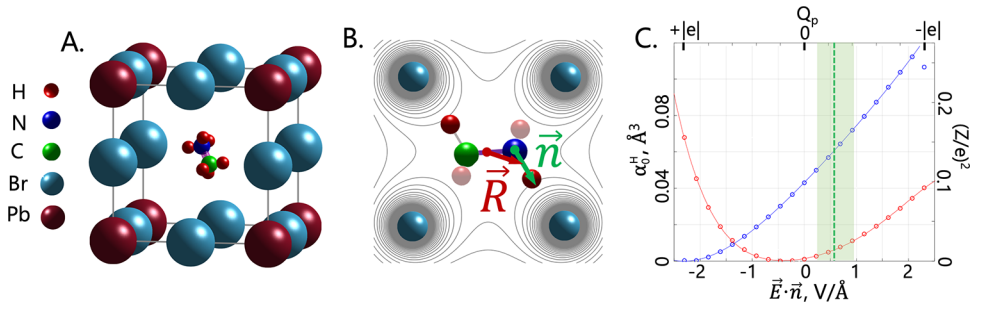

Figure 1. (A) Lattice structure of $MAPbBr_3$ (to scale). (B) Cartoon of the MA cation in the electrostatic field of the inorganic cage (not to scale); $\vec{n}$ is the unit vector along the bond direction; $\vec{R}$ is the distance to the center of the bond from the center of the lattice unit. (C) Static longitudinal polarizabilities α_0^H of C(N)−H bonds as a function of the electric field at the locus of the bond. For comparison, the field is also parametrized by the value of a point charge Q_p placed on the line connecting one of the H atoms to the neighboring N(C) atom, at a distance d = 2.5 Å from H. This d value corresponds to the most stable H−Br separation in the cubic phase of $MAPbBr_3$ for the N−H hydrogen[26,27] (for consistency, the same distance is chosen for C−H in our calculations). α_0^H is also parametrized with a square of the effective (Born) charge of an H atom, Z, as $\alpha_0^H = Z^2/m_H\Omega_H^2$ (see ref 28), where m_H is the mass of a hydrogen atom, and Ω_H is the resonant frequency of the C(N)−H stretching mode. The green dashed line (green rectangle) marks the estimated value (error margin) of the crystal field experienced by the C(N)−H bond (see the text for details).

applied electric field, $\vec{E}$, as $p_i(\omega) = \alpha_{ij}(\omega)E_j(\omega)$. Microscopically, $\vec{p}$ can be induced either by electron cloud polarization or by deformation of the molecule in question. When the field $\vec{E}$ becomes comparable to the interatomic one, the linear relation between $\vec{p}$ and $\vec{E}$ above is no longer valid and should be amended by assuming that α_{ij} depends on $\vec{E}$.[38] Such fields are natural for intracell lattice environments, meaning that even if the molecule retains its chemical autonomy within a compound, one should expect its vibrational polarizability to be noticeably affected by the local fields inside a lattice unit. This turns the polarizability of the molecule into a marker of these fields, which can be investigated in linear optical experiments, where probing fields are weak by definition.

Any molecular deformation can be decomposed into normal vibration modes,[39] where each normal mode k has a specific resonance frequency Ω_k and can be ascribed a frequency-dependent polarizability tensor $\alpha_{ij}^k(\omega)$. The sum of these terms determines the refractive index $n(\omega)$ of the medium; the contribution of each normal mode to n is the most prominent near its resonant frequency Ω_k.[40] In this work, we choose to focus on the vibration modes of methylammonium that correspond to the longitudinal displacement of the hydrogen atoms along the direction of the bond, $\vec{n}$, to the nearby N or C atoms (see Figure 1A,B). The main reason for this choice is that these modes are by far the strongest in terms of IR-intensity.[17,30,41] Elementary counting of the degrees of freedom reveals (in total) 6 modes that involve longitudinal stretching of the C(N)−H bond, which will be labeled as H_k or simply H.

The simplicity of methylammonium allows for a direct computation of the polarizability of the C(N)−H stretching mode, α_0^H, by means of density functional theory (DFT); for more details see ref 28. In Figure 1C we show how the (longitudinal) polarizabilities of the C−H and N−H bonds depend on the strength of the longitudinal electric field. To give these values some intuitive sense, the applied electric field at the locus of the C(N)−H bond is also parametrized by the charge Q_p of a point source located on the C(N)−H line at a distance d = 2.5 Å from the H atom; the value for d is motivated by the H−Br distance at room temperature.[26,27,42] Although, the present work focuses on the stoichiometric case, we note that our calculations indicate that the effect of localized lattice defects such as vacancies or color centers must be very significant. Indeed, the associated fields are on the order of $E_{def} \sim |e|/d^2 \sim 1$ V/Å in the vicinity of the molecule. They can renormalize bond polarizability by about 100%, meaning that the methylammonium cation can be a very sensitive probe of lattice imperfections.

The microscopic longitudinal bond polarizability α_{ij}^H depends on the fluctuating local crystal field $\vec{e}(\vec{R})$ (see Figure 1C). To relate it to the polarizability $\langle\alpha^H\rangle$ measured in experiment, α_{ij}^H must be averaged over all spatial orientations of the bond and different configurations of $\{\vec{e}(\vec{R})\}$. For $MAPbBr_3$, which is cubic (on average) at room temperature, one can write (see ref 28):

$$\langle\alpha^H\rangle = \frac{1}{3}\sum_{H_k=1}^{6}\int d\vec{X}\, d\vec{Q}\rho(\vec{X},\vec{Q})\alpha^{H_k}(\vec{X},\vec{Q}) \quad (1)$$

where the index H_k runs over the six longitudinal C(N)−H stretching modes (note that we assume that the polarizability of the molecule is the sum of polarizabilities of its bonds[43,44]); $\vec{X}$ ($\vec{Q}$) are the positions of atoms in the molecule (the cage); $\rho(\vec{X},\vec{Q})$ is the density matrix that determines probabilities of a specific lattice-molecule configuration given by $\vec{X}$ and $\vec{Q}$; $\alpha^{H_k}(\vec{X},\vec{Q})$ is the longitudinal polarizability of the H_kth bond in a configuration $\{\vec{X},\vec{Q}\}$ (here we rely on the Born−Oppenheimer approximation to assume that $\alpha^H(\vec{X},\vec{Q})$ only depends on instantaneous positions of atoms in the cage). To derive eq 1, we noted that according to our DFT calculations, $\alpha_{ij}^H(\vec{e}(\vec{R})) = \alpha^{H_k}(\vec{R})n_in_j$, where $\vec{n}$ is a unit vector along the bond direction, see ref 28 for further details.

The quantities ρ and α^H in eq 1 can be determined theoretically from the literature and DFT calculations for different scenarios, such as the presence of defects. Equation 1 relates these theoretical calculations to the measured average polarizability, $\langle\alpha^H\rangle$, allowing one to investigate microscopic properties of HOIPs using molecules as experimental probes.

To illustrate the formal discussion above, we proceed with measuring the average polarizability $\langle\alpha^H\rangle$ for a bulk single crystal sample of $MAPbBr_3$ in the cubic phase. For this purpose, we measure the group refractive index $n_g(\omega)$ in the mid-infrared frequency range relevant for vibrational degrees of freedom of methylammonium.[17] The advantage of the group

https://doi.org/10.1021/acs.jpclett.3c01158
J. Phys. Chem. Lett. 2023, 14, 6309−6314

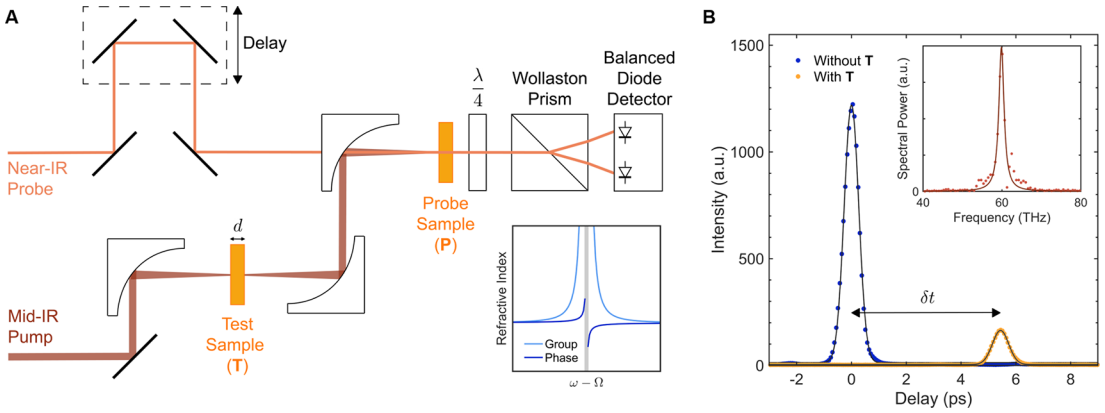

Figure 2. (A) Optical Kerr effect-based pump-probe method to obtain the group refractive index by measuring the time that it takes for a pulse to go through the test sample. The delay between the mid-IR pump and the near-IR probe is measured using balance detection of the mid-IR induced birefringence in the probe sample. The inset shows the region of anomalous dispersion for the phase and group refractive indexes, showing that the group refractive index is more divergent. (B) Example of measured signals of the pump-probe delay with and without test sample. The inset shows Fourier-transform infrared spectroscopy (FTIR) of the pump pulse.

index for probing molecular polarizability, which in general provides much weaker contribution to the refractive index as compared to the electronic one, lies in the fact that $n_g(\omega)$ features stronger divergence near resonances and is therefore more sensitive as compared to the phase index $n_{ph}(\omega)$. Indeed, $n_g(\omega)/n_{ph}(\omega) \approx \Omega/(\omega - \Omega)$ near the resonance frequency Ω (see the inset in Figure 2A).

To measure the group refractive index in a direct manner, we develop a time-resolved setup depicted in Figure 2A. The setup utilizes two samples of single-crystal $MAPbBr_3$: the actual test sample (**T** in Figure 2) in which n_g is measured and a probe sample for a broadband ultrafast detection of mid-infrared pulses by means of the optical Kerr effect (**P** in Figure 2). By measuring the time of arrival of the mid-IR pulse at the probe sample with and without the test sample, one obtains the delay δt introduced by the test sample. The time delay δt for the mid-IR pulse due to traveling through the perovskite sample of thickness d = 1.6 mm, is $\delta t = {}^{d}/_{c}(n_g - n_g^{air})$, where n_g and $n_g^{air} \approx 1$ are the group refractive indices of $MAPbBr_3$ and air, respectively; c is the speed of light.

The ultrafast optical Kerr effect in the probe sample is detected by the standard time-resolved pump-probe method in a balanced detection scheme (see Figure 2A and ref 28). An example of a time-resolved transient Kerr response for λ = 5 μm mid-IR pump with and without the test sample is depicted in Figure 2B. The difference in arrival time of the mid-IR pulse at the probe sample δt is measured as the distance between the two peak positions; the inset shows the FTIR of the pump pulse (see ref 28). Performing similar measurements for other mid-IR wavelength values, one can extract the perovskite group index $n_g(\omega) = n_g^{air} + c\delta t/d$ over a broad range of wavelengths.

The measured group refractive index dispersion $n_g(\omega)$ of bulk single crystal $MAPbBr_3$ as a function of the photon energy, $\hbar\omega$, is displayed in Figure 3. Here, we identify two regions of absorption, one in the low energy region at ~0.17 eV (1400 cm^{-1}) and another at a higher energy ~0.37 eV (3000 cm^{-1}), which can be associated with the bending and stretching modes of C(N)−H bonds, respectively.[17,30,41] The low value of extinction, κ, (see ref 28) in the region outside the immediate vicinity of the absorption band corresponding to the C(N)−H stretching modes justifies our assumption that these modes can be approximated as isolated from the nearby C(N)−H bending modes.

To extract the molecular contribution to the refractive index, we need to subtract the electronic contribution from the measured infrared $n_g(\omega)$. (Note that the electronic contribution to the refractive index is typically the dominant one, since electrons are much lighter than ions. Only close to a molecular resonance does the molecular contribution become important.) To this end, we use our previous measurements of the phase index in the visible and near-IR region.[45] In this high frequency range near the bulk band transition frequency, $\hbar\omega \sim \Delta_{gap}$ and the refractive index is determined by the electronic polarizability of the lead-halide cage. By first fitting the high-frequency phase index from ref 45 with a Sellmeier expression, and then calculating the group index from it and extrapolating the result to the mid-IR frequencies, one can obtain the electronic part $n_{g,el}(\omega)$ of the total group refractive index $n_g(\omega)$ coming from the crystal cage. $n_{g,el}(\omega)$ in the mid-IR range calculated this way is plotted as a light blue dashed line in Figure 3 providing an excellent fit to the data in the relevant frequency range away from the nearby absorption band. The molecular part of the group index $n_{g,mol}$ is found by subtracting the cage electronic contribution from the total refractive index: $n_{g,mol}(\omega) = n_g(\omega) - n_{g,el}(\omega)$ (see ref 28).

Once $n_{g,mol}(\omega)$ is known, it is possible to calculate the polarizability of the given mode by fitting it to the classical resonance profile near the resonant frequency. We focus on the C(N)−H stretching modes centered around $\hbar\Omega_H \approx 0.37$ eV (3000 cm^{-1}). Note that the resonance in Figure 3 corresponds not to a single mode but instead to a group of 6 different modes involving stretchings of different C(N)−H bonds. However, due to strong mass mismatch between H and C(N), the natural frequencies of these modes are very similar.[17,30,41] If we assume that C and N are infinitely heavy compared to hydrogen, then each vibration of H along the C(N)−H bond can be considered independent and decoupled from the rest. Within this approximation (that introduces an error of the order $\sim m_H/m_C \approx 10\%$), we shall use an oscillator model with a single resonant frequency (see the inset in Figure 3).

To connect $n_{g,mol}(\omega)$ to $\langle\alpha_0^H\rangle$, we account for the screening effect due to the polarizable cage and write in the vicinity of Ω_H (see ref 28 for derivation),

https://doi.org/10.1021/acs.jpclett.3c01158
J. Phys. Chem. Lett. 2023, 14, 6309−6314

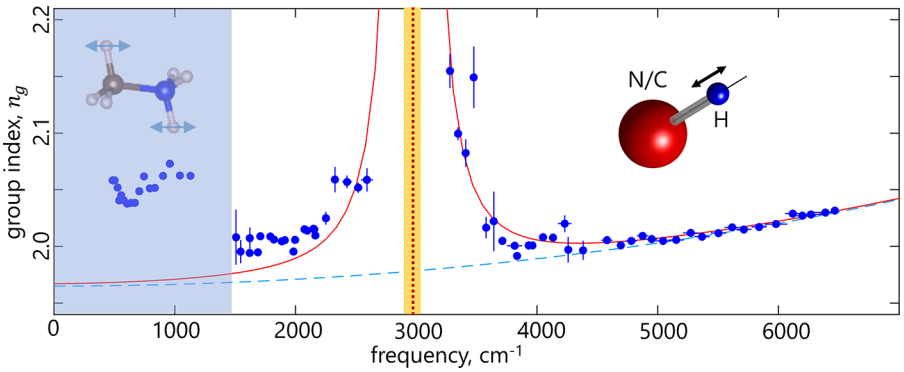

Figure 3. Group refractive index n_g measured using the setup depicted in Figure 2. The horizontal error bars are the full width at half-maximum (FWHM) of the FTIR calibration, and the vertical error bars are the FWHM of the dispersion from Figure 2B. The low-frequency region of vibrational resonances is indicated by the blue shading. Sketch of the corresponding (bending) molecular modes is presented in the shaded region. The right inset is an illustration of a longitudinal C(N)−H bond stretching, representing the entire cluster of 6 stretching modes in the energy region around 3000 cm^{-1}. The solid red line is the fit according to eq 2; the vertical red dotted line marks the resonant frequency, Ω_H, from the fit; the light blue dashed curve is the electronic group index obtained from the Sellmeier fit to the high energy data of ref 45; the yellow shaded region illustrates the frequency spread within the longitudinal-stretching mode cluster.[17,30,41,46]

$$n_{g,\mathrm{mol}}(\omega) \approx \langle \alpha_0^H \rangle \frac{4\pi N}{3} \frac{(\overline{n}_{\mathrm{el}}^2 + 2)^2}{12\overline{n}_{\mathrm{el}}} \cdot \frac{\Omega_H^2}{(\Omega_H - \omega)^2} \qquad (2)$$

where $\overline{n}_{\mathrm{el}} \equiv n_{\mathrm{ph,el}}(\Omega_H)$ is the electronic contribution of the phase refractive index at Ω_H, and $\langle \alpha_0^H \rangle$ is the average static (longitudinal) polarizability of the C(N)−H bond. The solid line in Figure 3 is the result of the fit of $n_{g,\mathrm{mol}}(\omega)$ to the expression in eq 2. From the fit, we obtain $\langle \alpha_0^H \rangle \approx (7.0 \pm 1.1) \times 10^{-2}$ Å^3, with the error representing the 95% confidence range. Since the fitting error significantly exceeds the spread in resonant frequency values for C(N)−H stretching modes (∼10%, see above) one can neglect the latter for the sake of discussion.

With an experimental value for $\langle \alpha^H \rangle$ at hand, we compare it with that of eq 1 to see what can be said about the interaction between MA and the surrounding cage. In the simplest case, one may note that in some molecular dynamics studies the C−N axis of the cation appears to explore the available space quasi-uniformly[47,48] and naively assume that the molecule rotations are uncorrelated with the inorganic cage. In terms of eq 1, this limit corresponds to $\rho(\vec{X}, \vec{Q}) = \rho_{\mathrm{mol}}(\vec{X})\rho_{\mathrm{cage}}(\vec{Q})$, for which (see ref 28) the average polarizability remains unrenormalized even in the presence of strong crystal fields

$$\langle \alpha_0^H \rangle_{\mathrm{uncorr}} = \alpha_0^{H_N}(\vec{E} = 0) + \alpha_0^{H_C}(\vec{E} = 0)$$

where $\alpha_0^H(E = 0)$ can be taken from Figure 1C so that $\langle \alpha_0^H \rangle_{\mathrm{uncorr}} \approx 4.4 \times 10^{-2}$ Å^3. Since the discrepancy between this value and the experimental one above is beyond the error margin of our approach, we can conclusively rule out uncorrelated molecule-cage dynamics, in agreement with prior results.[26,49−51] If, conversely, we fix the density matrix in eq 1 in accordance with previous reports in the literature,[28] then we arrive at the value for the local crystal field experienced by the N−H bond $|E_{\mathrm{CF}}| = (0.6 \pm 0.3)$ V/Å by comparing the polarizabilities in Figure 1C with experimental values.

Note that in a stoichiometric lattice the Coulombic fields coming from the atoms, if treated as point sources, cancel each other very finely inside the lattice cell (see ref 28). Therefore, to account for the relatively large value of E_{CF}, we need to go beyond the point-source approximation for the atoms in the inorganic cage. The lowest-order multipole moment would be the quadrupolar moment D of the bromine atom with the axis along Pb−Br−Pb. Knowing $|E_{\mathrm{CF}}|$ and the distance between H and Br one can estimate that $D \sim +1$ eÅ^2. Recalling now that a hydrogen bond can be defined as an interaction between H and a multipole potential of a neighboring atom,[52] we estimate it from the energy of the H−Br electrostatic interaction $\mathcal{E}_H \sim 0.1$ eV (for more details, see ref 28). This value is in reasonable agreement with previous estimates[50,53] of the energy of the H−Br hydrogen bond, illustrating that the proposed here molecular probe can provide important insight into the existence of hydrogen bonding in HOIPs.[54,55]

In conclusion, we propose the semiautonomous A-site cations in HOIPs as a sensitive local probe for optical spectroscopy, which complements the existing techniques such as NMR and NQR. To illustrate the formulated theoretical framework, we have analyzed the average polarizability of the N−H stretching mode extracted by measuring the group refractive index of a bulk single crystal sample of $MAPbBr_3$ in the mid-IR wavelength range. Based on the analysis, we have ruled out the possibility of an uncorrelated motion of methylammonium cation in a PbBr cage and estimated local electric fields at the locus of the C(N)−H bond. We also estimated the value of the quadrupole moment for the Br atom, and the energy of the H−Br hydrogen bond. Our work proposes a new approach to the study of the complex behavior of the dynamically disordered inorganic cage, which will provide novel insight into fundamental properties of lead-halide perovskites. In particular, being all-optical, our approach can be employed to study ultrafast transient behavior of lattice irregularities, for example polaronic structures formed around photoexcitations. Since it is widely expected that the formation of such polarons underlies some most important optoelectronic properties of lead halide perovskites,[10] our results offer an approach to clarify some of the most pressing questions related to the solar energy harvesting applications of lead-halide perovskites.

■ ASSOCIATED CONTENT

Supporting Information

The Supporting Information is available free of charge at https://pubs.acs.org/doi/10.1021/acs.jpclett.3c01158.

https://doi.org/10.1021/acs.jpclett.3c01158
J. Phys. Chem. Lett. 2023, 14, 6309−6314

Additional experimental and theoretical details including description of methods. Derivation of equations and quantities discussed in the main text (PDF)

AUTHOR INFORMATION

Corresponding Author

Zhanybek Alpichshev − *Institute of Science and Technology Austria (ISTA), 3400 Klosterneuburg, Austria*; Email: alpishev@ist.ac.at

Authors

Yujing Wei − *Institute of Science and Technology Austria (ISTA), 3400 Klosterneuburg, Austria*; Present Address: Department of Chemistry, Columbia University, New York, New York 10027, United States; orcid.org/0000-0001-8913-9719

Artem G. Volosniev − *Institute of Science and Technology Austria (ISTA), 3400 Klosterneuburg, Austria*

Dusan Lorenc − *Institute of Science and Technology Austria (ISTA), 3400 Klosterneuburg, Austria*

Ayan A. Zhumekenov − *KAUST Catalysis Center (KCC), Division of Physical Sciences and Engineering, King Abdullah University of Science and Technology (KAUST), Thuwal 23955-6900, Kingdom of Saudi Arabia*; Present Address: School of Materials Science and Engineering, Nanyang Technological University, 50 Nanyang Avenue, 639798 Singapore.; orcid.org/0000-0002-3216-5315

Osman M. Bakr − *KAUST Catalysis Center (KCC), Division of Physical Sciences and Engineering, King Abdullah University of Science and Technology (KAUST), Thuwal 23955-6900, Kingdom of Saudi Arabia*; orcid.org/0000-0002-3428-1002

Mikhail Lemeshko − *Institute of Science and Technology Austria (ISTA), 3400 Klosterneuburg, Austria*

Complete contact information is available at: https://pubs.acs.org/10.1021/acs.jpclett.3c01158

Author Contributions

‡Y.W. and A.G.V. contributed equally.

Notes

The authors declare no competing financial interest.

ACKNOWLEDGMENTS

We thank Bingqing Cheng and Hong-Zhou Ye for valuable discussions; Y.W.'s work at IST Austria was supported through ISTernship summer internship program funded by OeAD-GmbH; D.L. and Z.A. acknowledge support by IST Austria (ISTA); M.L. acknowledges support by the European Research Council (ERC) Starting Grant No. 801770 (ANGULON). A.A.Z. and O.M.B. acknowledge support by KAUST.

REFERENCES

(1) Min, H.; Lee, D. Y.; Kim, J.; Kim, G.; Lee, K. S.; Kim, J.; Paik, M. J.; Kim, Y. K.; Kim, K. S.; Kim, M. G.; Shin, T. J.; Il Seok, S. Perovskite solar cells with atomically coherent interlayers on SnO_2 electrodes. *Nature* **2021**, *598*, 444−450.

(2) Almora, O.; et al. Device Performance of Emerging Photovoltaic Materials (Version 3). *Adv. Energy Mater.* **2023**, *13*, 2203313.

(3) Dong, Q.; Fang, Y.; Shao, Y.; Mulligan, P.; Qiu, J.; Cao, L.; Huang, J. Electron-hole diffusion lengths 175 μm in solution-grown $CH_3NH_3PbI_3$ single crystals. *Science* **2015**, *347*, 967−970.

(4) Turedi, B.; et al. Single-Crystal Perovskite Solar Cells Exhibit Close to Half A Millimeter Electron-Diffusion Length. *Adv. Mater.* **2022**, *34*, 2202390.

(5) Shi, D.; et al. Low trap-state density and long carrier diffusion in organolead trihalide perovskite single crystals. *Science* **2015**, *347*, 519−522.

(6) Xing, G.; Mathews, N.; Sun, S.; Lim, S. S.; Lam, Y. M.; Grätzel, M.; Mhaisalkar, S.; Sum, T. C. Long-Range Balanced Electron- and Hole-Transport Lengths in Organic-Inorganic $CH_3NH_3PbI_3$. *Science* **2013**, *342*, 344−347.

(7) Brenner, T. M.; Egger, D. A.; Kronik, L.; Hodes, G.; Cahen, D. Hybrid organic—inorganic perovskites: low-cost semiconductors with intriguing charge-transport properties. *Nat. Rev. Mater.* **2016**, *1*, 15007.

(8) Stranks, S. D.; Eperon, G. E.; Grancini, G.; Menelaou, C.; Alcocer, M. J. P.; Leijtens, T.; Herz, L. M.; Petrozza, A.; Snaith, H. J. Electron-Hole Diffusion Lengths Exceeding 1 Micrometer in an Organometal Trihalide Perovskite Absorber. *Science* **2013**, *342*, 341−344.

(9) Lekesi, L. P.; Koao, L. F.; Motloung, S. V.; Motaung, T. E.; Malevu, T. Developments on Perovskite Solar Cells (PSCs): A Critical Review. *Appl. Sci.* **2022**, *12*, 672.

(10) Miyata, K.; Meggiolaro, D.; Trinh, M. T.; Joshi, P. P.; Mosconi, E.; Jones, S. C.; Angelis, F. D.; Zhu, X.-Y. Large polarons in lead halide perovskites. *Sci. Adv.* **2017**, *3*, No. e1701217.

(11) Yin, W.-J.; Shi, T.; Yan, Y. Unusual defect physics in $CH_3NH_3PbI_3$ perovskite solar cell absorber. *Appl. Phys. Lett.* **2014**, *104*, 063903.

(12) Zhu, X.-Y.; Podzorov, V. Charge Carriers in Hybrid Organic−Inorganic Lead Halide Perovskites Might Be Protected as Large Polarons. *J. Phys. Chem. Lett.* **2015**, *6*, 4758−4761.

(13) Zhu, H.; Miyata, K.; Fu, Y.; Wang, J.; Joshi, P. P.; Niesner, D.; Williams, K. W.; Jin, S.; Zhu, X.-Y. Screening in crystalline liquids protects energetic carriers in hybrid perovskites. *Science* **2016**, *353*, 1409−1413.

(14) Frost, J. M.; Butler, K. T.; Brivio, F.; Hendon, C. H.; van Schilfgaarde, M.; Walsh, A. Atomistic Origins of High-Performance in Hybrid Halide Perovskite Solar Cells. *Nano Lett.* **2014**, *14*, 2584−2590.

(15) Koutentakis, G. M.; Ghazaryan, A.; Lemeshko, M. Rotor Lattice Model of Ferroelectric Large Polarons. *arXiv* **2023**, 2301.09875 v2.

(16) Kang, J.; Wang, L.-W. High Defect Tolerance in Lead Halide Perovskite $CsPbBr_3$. *J. Phys. Chem. Lett.* **2017**, *8*, 489−493.

(17) Leguy, A. M. A.; Goñi, A. R.; Frost, J. M.; Skelton, J.; Brivio, F.; Rodríguez-Martínez, X.; Weber, O. J.; Pallipurath, A.; Alonso, M. I.; Campoy-Quiles, M.; Weller, M. T.; Nelson, J.; Walsh, A.; Barnes, P. R. F. Dynamic disorder, phonon lifetimes, and the assignment of modes to the vibrational spectra of methylammonium lead halide perovskites. *Phys. Chem. Chem. Phys.* **2016**, *18*, 27051−27066.

(18) Ferreira, A.; Létoublon, A.; Paofai, S.; Raymond, S.; Ecolivet, C.; Rufflé, B.; Cordier, S.; Katan, C.; Saidaminov, M.; Zhumekenov, A.; Bakr, O.; Even, J.; Bourges, P. Elastic Softness of Hybrid Lead Halide Perovskites. *Phys. Rev. Lett.* **2018**, *121*, 085502.

(19) Ferreira, A. C.; Paofai, S.; Létoublon, A.; Ollivier, J.; Raymond, S.; Hehlen, B.; Rufflé, B.; Cordier, S.; Katan, C.; Even, J.; Bourges, P. Direct evidence of weakly dispersed and strongly anharmonic optical phonons in hybrid perovskites. *Commun. Phys.* **2020**, *3*, 48.

(20) Lanigan-Atkins, T.; He, X.; Krogstad, M. J.; Pajerowski, D. M.; Abernathy, D. L.; Xu, G. N. M. N.; Xu, Z.; Chung, D.-Y.; Kanatzidis, M. G.; Rosenkranz, S.; Osborn, R.; Delaire, O. Two-dimensional overdamped fluctuations of the soft perovskite lattice in $CsPbBr_3$. *Nat. Mater.* **2021**, *20*, 977−983.

(21) Yaffe, O.; Guo, Y.; Tan, L. Z.; Egger, D. A.; Hull, T.; Stoumpos, C. C.; Zheng, F.; Heinz, T. F.; Kronik, L.; Kanatzidis, M. G.; Owen, J. S.; Rappe, A. M.; Pimenta, M. A.; Brus, L. E. Local Polar Fluctuations in Lead Halide Perovskite Crystals. *Phys. Rev. Lett.* **2017**, *118*, 136001.

(22) Songvilay, M.; Giles-Donovan, N.; Bari, M.; Ye, Z.-G.; Minns, J. L.; Green, M. A.; Xu, G.; Gehring, P. M.; Schmalzl, K.; Ratcliff, W. D.; Brown, C. M.; Chernyshov, D.; van Beek, W.; Cochran, S.; Stock, C.

Common acoustic phonon lifetimes in inorganic and hybrid lead halide perovskites. *Phys. Rev. Mater.* **2019**, *3*, 093602.
(23) Peng, W.; Aranda, C.; Bakr, O. M.; Garcia-Belmonte, G.; Bisquert, J.; Guerrero, A. Quantification of Ionic Diffusion in Lead Halide Perovskite Single Crystals. *ACS Energy Lett.* **2018**, *3*, 1477−1481.
(24) Whalley, L. D.; Frost, J. M.; Jung, Y.-K.; Walsh, A. Perspective: Theory and simulation of hybrid halide perovskites. *J. Chem. Phys.* **2017**, *146*, 220901.
(25) Mozur, E. M.; Neilson, J. R. Cation Dynamics in Hybrid Halide Perovskites. *Annu. Rev. Mater. Res.* **2021**, *51*, 269−291.
(26) Yin, T.; Fang, Y.; Fan, X.; Zhang, B.; Kuo, J.-L.; White, T. J.; Chow, G. M.; Yan, J.; Shen, Z. X. Hydrogen-Bonding Evolution during the Polymorphic Transformations in $CH_3NH_3PbBr_3$: Experiment and Theory. *Chem. Mater.* **2017**, *29*, 5974−5981.
(27) Varadwaj, A.; Varadwaj, P. R.; Marques, H. M.; Yamashita, K. Halogen in materials design: Revealing the nature of hydrogen bonding and other non-covalent interactions in the polymorphic transformations of methylammonium lead tribromide perovskite. *Mater. Today Chem.* **2018**, *9*, 1−16.
(28) Supplemenatry Information.
(29) Filippetti, A.; Mattoni, A. Hybrid perovskites for photovoltaics: Insights from first principles. *Phys. Rev. B* **2014**, *89*, 125203.
(30) Pérez-Osorio, M. A.; Milot, R. L.; Filip, M. R.; Patel, J. B.; Herz, L. M.; Johnston, M. B.; Giustino, F. Vibrational Properties of the Organic−Inorganic Halide Perovskite $CH_3NH_3PbI_3$ from Theory and Experiment: Factor Group Analysis, First-Principles Calculations, and Low-Temperature Infrared Spectra. *J. Phys. Chem. C* **2015**, *119*, 25703−25718.
(31) Mattoni, A.; Filippetti, A.; Caddeo, C. Modeling hybrid perovskites by molecular dynamics. *J. Phys.: Condens. Matter* **2017**, *29*, 043001.
(32) Govinda, S.; Kore, B. P.; Bokdam, M.; Mahale, P.; Kumar, A.; Pal, S.; Bhattacharyya, B.; Lahnsteiner, J.; Kresse, G.; Franchini, C.; Pandey, A.; Sarma, D. D. Behavior of Methylammonium Dipoles in $MAPbX_3$ (X = Br and I). *J. Phys. Chem. Lett.* **2017**, *8*, 4113−4121.
(33) Senocrate, A.; Moudrakovski, I.; Maier, J. Short-range ion dynamics in methylammonium lead iodide by multinuclear solid state NMR and ^{127}I NQR. *Phys. Chem. Chem. Phys.* **2018**, *20*, 20043−20055.
(34) Piveteau, L.; et al. Bulk and Nanocrystalline Cesium Lead-Halide Perovskites as Seen by Halide Magnetic Resonance. *ACS Cent. Sci.* **2020**, *6*, 1138−1149.
(35) Piveteau, L.; Morad, V.; Kovalenko, M. V. Solid-State NMR and NQR Spectroscopy of Lead-Halide Perovskite Materials. *J. Am. Chem. Soc.* **2020**, *142*, 19413−19437.
(36) Barth, A. Infrared spectroscopy of proteins. *Biochim. Biophys. Acta, Bioenerg.* **2007**, *1767*, 1073−1101.
(37) Ma, J.; Pazos, I. M.; Zhang, W.; Culik, R. M.; Gai, F. Site-Specific Infrared Probes of Proteins. *Annu. Rev. Phys. Chem.* **2015**, *66*, 357−377.
(38) Boyd, R. W. Order-of-magnitude estimates of the nonlinear optical susceptibility. *J. Mod. Opt.* **1999**, *46*, 367−378.
(39) Landau, L. D.; Lifshitz, E. M. *Mechanics*, 3rd ed.; Course of Theoretical Physics; Butterworth-Heinemann, 1976; Vol. *1*.
(40) Born, M.; Wolf, E. *Principles of Optics*; Cambridge University Press, 2019.
(41) Pérez-Osorio, M. A.; Lin, Q.; Phillips, R. T.; Milot, R. L.; Herz, L. M.; Johnston, M. B.; Giustino, F. Raman Spectrum of the Organic−Inorganic Halide Perovskite $CH_3NH_3PbI_3$ from First Principles and High-Resolution Low-Temperature Raman Measurements. *J. Phys. Chem. C* **2018**, *122*, 21703−21717.
(42) Abia, C.; López, C. A.; Cañadillas-Delgado, L.; Fernández-Diaz, M. T.; Alonso, J. A. Crystal structure thermal evolution and novel orthorhombic phase of methylammonium lead bromide, $CH_3NH_3PbBr_3$. *Sci. Rep.* **2022**, *12*, 18647.
(43) Denbigh, K. G. The polarisabilities of bonds. *Trans. Faraday Soc.* **1940**, *36*, 936−948.
(44) Le Févre, R. In *Molecular Refractivity and Polarizability*; Advances in Physical Organic Chemistry; Gold, V., Ed.; Academic Press, 1965; Vol. *3*, pp 1−90.
(45) Volosniev, A. G.; Shiva Kumar, A.; Lorenc, D.; Ashourishokri, Y.; Zhumekenov, A. A.; Bakr, O. M.; Lemeshko, M.; Alpichshev, Z. Spin-Electric Coupling in Lead Halide Perovskites. *Phys. Rev. Lett.* **2023**, *130*, 106901.
(46) Schuck, G.; Többens, D. M.; Koch-Müller, M.; Efthimiopoulos, I.; Schorr, S. Infrared Spectroscopic Study of Vibrational Modes across the Orthorhombic−Tetragonal Phase Transition in Methylammonium Lead Halide Single Crystals. *J. Phys. Chem. C* **2018**, *122*, 5227−5237.
(47) Mattoni, A.; Filippetti, A.; Saba, M. I.; Delugas, P. Methylammonium Rotational Dynamics in Lead Halide Perovskite by Classical Molecular Dynamics: The Role of Temperature. *J. Phys. Chem. C* **2015**, *119*, 17421−17428.
(48) Gallop, N. P.; Selig, O.; Giubertoni, G.; Bakker, H. J.; Rezus, Y. L. A.; Frost, J. M.; Jansen, T. L. C.; Lovrincic, R.; Bakulin, A. A. Rotational Cation Dynamics in Metal Halide Perovskites: Effect on Phonons and Material Properties. *J. Phys. Chem. Lett.* **2018**, *9*, 5987−5997.
(49) Leguy, A.; Frost, J.; McMahon, A.; et al. The dynamics of methylammonium ions in hybrid organic−inorganic perovskite solar cells. *Nat. Commun.* **2015**, *6*, 7124.
(50) Svane, K. L.; Forse, A. C.; Grey, C. P.; Kieslich, G.; Cheetham, A. K.; Walsh, A.; Butler, K. T. How Strong Is the Hydrogen Bond in Hybrid Perovskites? *J. Phys. Chem. Lett.* **2017**, *8*, 6154−6159.
(51) Saleh, G.; Biffi, G.; Di Stasio, F.; Martín-García, B.; Abdelhady, A. L.; Manna, L.; Krahne, R.; Artyukhin, S. Methylammonium Governs Structural and Optical Properties of Hybrid Lead Halide Perovskites through Dynamic Hydrogen Bonding. *Chem. Mater.* **2021**, *33*, 8524−8533.
(52) Arunan, E.; Desiraju, G. R.; Klein, R. A.; Sadlej, J.; Scheiner, S.; Alkorta, I.; Clary, D. C.; Crabtree, R. H.; Dannenberg, J. J.; Hobza, P.; Kjaergaard, H. G.; Legon, A. C.; Mennucci, B.; Nesbitt, D. J. Definition of the hydrogen bond (IUPAC Recommendations 2011). *Pure Appl. Chem.* **2011**, *83*, 1637−1641.
(53) Lee, J. H.; Lee, J.-H.; Kong, E.-H.; Jang, H. M. The nature of hydrogen-bonding interaction in the prototypic hybrid halide perovskite, tetragonal $CH_3NH_3PbI_3$. *Sci. Rep.* **2016**, *6*, 21687.
(54) Glaser, T.; Müller, C.; Sendner, M.; Krekeler, C.; Semonin, O. E.; Hull, T. D.; Yaffe, O.; Owen, J. S.; Kowalsky, W.; Pucci, A.; Lovrinčić, R. Infrared Spectroscopic Study of Vibrational Modes in Methylammonium Lead Halide Perovskites. *J. Phys. Chem. Lett.* **2015**, *6*, 2913−2918.
(55) Ibaceta-Jaña, J.; Chugh, M.; Novikov, A. S.; Mirhosseini, H.; Kühne, T. D.; Szyszka, B.; Wagner, M. R.; Muydinov, R. Do Lead Halide Hybrid Perovskites Have Hydrogen Bonds? *J. Phys. Chem. C* **2022**, *126*, 16215−16226.

https://doi.org/10.1021/acs.jpclett.3c01158
J. Phys. Chem. Lett. 2023, 14, 6309−6314